ADVANCED FUNCTIONAL MATERIALS
www.afm-journal.de

Design of an Artificial Peptide Inspired by Transmembrane Mitochondrial Protein for Escorting Exogenous DNA into the Mitochondria to Restore their Functions by Simultaneous Multiple Gene Expression

*Naoto Yoshinaga, Takaaki Miyamoto, Masaki Odahara, Noriko Takeda-Kamiya, Kiminori Toyooka, Seia Nara, Haruna Nishimura, Feng Ling, Masayuki Su'etsugu, Minoru Yoshida, and Keiji Numata**

Mitochondria are vital organelles regulating essential cellular functions. Human mitochondrial DNA (mtDNA) consists of 37 genes, 13 of which encode mitochondrial proteins, and the remaining 24 genes encode two ribosomal RNAs and 22 transfer RNAs needed for the translation of the mtDNA-encoded 13 proteins. However, mtDNA often impairs the expression and function of these genes due to various mutations, ultimately causing mitochondrial dysfunction. To recover from this desperate condition, developing the technology to supply all mitochondrial proteins encoded by mtDNA at once is an urgent task, but there is no established strategy for this purpose. In this study, a simple yet effective mitochondrial gene delivery system is proposed comprising an artificial peptide inspired by a transmembrane mitochondrial membrane protein. The designed mitochondria-targeting peptides presented on the carrier surface effectively guide the encapsulated plasmid to the mitochondria, facilitating mitochondrial uptake and gene expression. The developed system successfully delivers exogenous mtDNA to mtDNA-depleted cells and leads to simultaneous multigene expression, ultimately restoring mitochondrial functions, including the mitochondrial respiration rate. The established multiple gene expression system in each mitochondrion is a game-changing technology that can accelerate the development of mitochondrial engineering technologies as well as clinical applications for mitochondrial diseases.

1. Introduction

Mitochondria play essential roles in cellular functions, such as energy production.[1] Their own genome, mitochondrial DNA (mtDNA), which encodes 13 distinct and essential proteins for oxidative phosphorylation, supports these vital functions by providing these proteins along with the nuclear genome.[2] Pathogenic mutations related to mitochondrial proteins or RNAs cause mitochondrial diseases.[3] mtDNA undergoes genomic mutation more frequently than nuclear DNA.[4] Increased genetic variation in mtDNA, called heteroplasmic conditions, reduces proper mitochondrial gene expression, leading to mitochondrial disorders when the ratio of mutant mtDNA exceeds a threshold.[5] For example, a single mutation in the mitochondrial ATP6 gene (m.8993T > G or >C) causes neuropathy, ataxia, and pigmentary retinopathy,[6] and large deletion of mtDNA causes maternally inherited diabetes and deafness and Kearns–Sayre syndrome.[7] There is a pressing demand

N. Yoshinaga, T. Miyamoto, M. Odahara, K. Numata
Biomacromolecule Research Team
RIKEN Center for Sustainable Resource Science
Wako-shi, Saitama 351-0198, Japan
E-mail: keiji.numata@riken.jp

The ORCID identification number(s) for the author(s) of this article can be found under https://doi.org/10.1002/adfm.202306070

[+]Present address: OriCiro Genomics, Inc., Tokyo 113-8485, Japan

DOI: 10.1002/adfm.202306070

N. Yoshinaga, K. Numata
Institute for Advanced Biosciences
Keio University
Tsuruoka-shi, Yamagata 997-0017, Japan

N. Takeda-Kamiya, K. Toyooka
Technology Platform Division
Mass Spectrometry and Microscopy Unit
RIKEN Center for Sustainable Resource Science
Yokohama-shi, Kanagawa 230-0045, Japan

S. Nara[+], M. Su'etsugu
Department of Life Science
College of Science
Rikkyo University
Toshima-ku, Tokyo 171-8501, Japan

to develop methodologies regulating the gene expression in the mitochondria to elucidate the complicated mitochondrial conditions and eventually advance genetic therapeutics for mitochondrial diseases.

Introducing exogenous DNA into the mitochondria is one of the most straightforward approaches to regulating mitochondrial gene expression. For decades, tremendous efforts have been devoted to developing effective way to deliver genes into the mitochondria.[8] The decoration of delivery carriers with mitochondria-targeting sequences (MTSs) is the most powerful way to enhance mitochondria-targeting efficiency. Adeno-associated virus (AAV) with an MTS is a good example of an MTS-based system, accomplishing sufficient mitochondrial expression of ubiquinone oxidoreductase (NADH) subunit IV,[9] which is encoded by mtDNA. However, AAV can load up to 5 kbp DNA, which is far from delivering large DNA molecules encoding multiple genes, such as mtDNA, to improve heteroplasmic conditions. The difficult preparation process of MTS-installed AAV also restricts the applicational use of this system. Therefore, developing sophisticated carriers for secured gene delivery into the mitochondria is still needed to establish mitochondrial engineering *ad arbitrium*.

We envisioned that a much simpler strategy using an MTS could achieve multiple, efficient gene expressions in the mitochondria. Here, we report a potential mitochondria-targeting gene delivery system based on a novel synthetic peptide. We selected as an MTS the 32 N-terminal amino acid residues of the natural mitoNEET protein (108 amino acids), which is an outer mitochondrial membrane protein regulating the biogenesis of cells by sensing ROS and contains a transmembrane sequence between amino acids 14 and 32.[10] The mitochondrial outer membrane protein relevant to protein import can recognize the N-terminal signal transmembrane sequence, which is expected to lead to an efficient accumulation of encapsulated genes in the mitochondria. A fusion protein of GFP with the N-terminal half of mitoNEET protein exhibited convincing accumulation in the mitochondria.[11] To effectively encapsulate genes, the N-terminal 32 amino acid sequence of mitoNEET protein was fused with nine arginine-histidine (RH) or lysine-histidine (KH) repeats as a cationic segment (mitoNEET-$(RH)_9$ and mitoNEET-$(KH)_9$). The positively charged arginine or lysine residues bind to genes through electrostatic interactions, inducing polyplex formation. Encapsulation in polyplexes equipped with mitoNEET sequence may allow plasmid to enter the cells due to the surface positive charge and to be guided to the mitochondria. Additionally, histidine residues can enhance the endosomal escape of the polyplexes.[12] The rationally designed polyplexes successfully guided the encapsulated genes into the mitochondria by the same recognition pathway as the natural mitoNEET protein. The reached polyplexes were surely internalized into the mitochondria, enhancing mitochondria-specific gene expression. As a model experiment to engineer mitochondria, we attempted to recover mitochondrial function in an mtDNA-depleted cell line (ρ^0 cell) by introducing exogenous mtDNA, which is difficult to be delivered into the mitochondria by conventional systems due to its large size (16.7 kbp). The mtDNA transfected by the mitoNEET polyplexes performed multiple gene expressions and consequently improved the mitochondrial energy production in ρ^0 cells, demonstrating the feasibility of mitochondrial engineering by simultaneously supplying several proteins through a simple procedure for the first time.

2. Results

2.1. Preparation of Mitochondria-Targeting Polyplexes with a Suitable Secondary Structure and Low Cytotoxicity

Efficient mitochondria-targeting requires low cytotoxicity and a suitable secondary structure, α-helix.[13] We designed two polyplexes composed of synthetic peptides with different cationic segments. Polyplexes were prepared from plasmid and the peptides with mitoNEET (MSLTSSSSVRVEWIAAVTIAAGTAAIGYLAYK) and a cationic segment, -$(RH)_9$ or -$(KH)_9$, by mixing in aqueous solution at various residual molar ratios between amine and guanidine groups on the peptides (N) and phosphate groups on plasmids (P) (N/P ratio). Dynamic light scattering (DLS) measurements revealed that the mixture of the peptide and plasmid at N/P ratios of 2, 2.5, 3, and 4 showed a 64–88 nm cumulant diameter with a relatively narrow size distribution, while samples prepared at an N/P ratio of 1 formed aggregates due to the complete charge neutralization between carrier components (**Table 1**). These results indicate successful polyplex formation at N/P ratios of 2, 2.5, 3, and 4. The conversion of surface ζ-potential from negative to positive over an N/P ratio of 1.5 supports the complexation of plasmids by mitoNEET-$(RH)_9$ and mitoNEET-$(KH)_9$. The positively-charged surface may facilitate cellular uptake due to the electrostatic interaction with the cell surface.[14] While no considerable difference in DLS measurements was observed between the two cationic sequences, mitoNEET-$(RH)_9$ and mitoNEET-$(KH)_9$, the circular dichroism (CD) measurements showed an interesting difference (**Figure 1**a,b). In mitoNEET-$(RH)_9$ polyplexes prepared at an N/P ratio of 2, 78% of the peptides formed an α-helical structure. In contrast, the secondary structure of the mitoNEET-$(KH)_9$ peptide in polyplexes consisted of random coil (56%) and α-helix (41%). Interestingly, the free peptides and polyplexes prepared at an N/P ratio of 0.5 consisted of various secondary structures (Figure 1b; Figure S1, Supporting Information). Probably charge repulsion between cationic residues on the peptides and the uncondensed condition of plasmid disturbed the formation of α-helical structure in the mitoNEET sequence. These results indicated the potential of the mitoNEET-$(RH)_9$ peptide

H. Nishimura, F. Ling, M. Yoshida
Chemical Genomics Research Group
RIKEN Center for Sustainable Resource Science
Wako-shi, Saitama 351-0198, Japan
M. Yoshida
Department of Biotechnology
Graduate School of Agricultural and Life Sciences
and Collaborative Research Institute for Innovative Microbiology
The University of Tokyo
Bunkyo-ku, Tokyo 113-8657, Japan
K. Numata
Department of Material Chemistry
Kyoto University
Kyoto-shi, Kyoto 606-8501, Japan

Table 1. Characteristics of mitoNEET polyplexes. Data are shown as the mean ± SEM ($n = 4$).

	N/P ratio					
	1	1.5	2	2.5	3	4
			mitoNEET-$(RH)_9$ polyplex			
Size	2528 ± 345 nm	517 ± 159 nm	78 ± 2.4 nm	76 ± 3.0 nm	83 ± 2.9 nm	88 ± 6.9 nm
PDI	0.33 ± 0.01	0.29 ± 0.02	0.22 ± 0.01	0.24 ± 0.02	0.24 ± 0.01	0.22 ± 0.02
ζ-potential	−18.9 ± 2.0 mV	+13.9 ± 0.5 mV	+21.4 ± 2.9 mV	+21.4 ± 2.9 mV	+19.7 ± 2.1 mV	+20.1 ± 4.2 mV
			mitoNEET-$(KH)_9$ polyplex			
Size	1205 ± 78 nm	64 ± 0.6 nm	67 ± 1.6 nm	77 ± 9.2 nm	65 ± 1.0 nm	64 ± 2.2 nm
PDI	0.35 ± 0.03	0.18 ± 0.02	0.16 ± 0.02	0.18 ± 0.01	0.17 ± 0.01	0.20 ± 0.01
ζ-potential	−7.4 ± 1.1 mV	+27.2 ± 1.4 mV	+29.0 ± 2.6 mV	+24.7 ± 1.0 mV	+28.3 ± 1.2 mV	+28.5 ± 0.7 mV

in polyplexes at an N/P ratio of 2 for efficient mitochondria-targeting.

The difference in cationic sequences also affected the stability of polyplexes to tolerate polyion exchange reactions. The structural robustness of polyplexes against competitive anionic macromolecules is an important factor in avoiding polyplex dissociation during delivery process for efficient cellular uptake.[15] In the presence of a competitive polyanion, dextran sulfate, with a residual molar ratio between anionic charges on dextran sulfate (A) and phosphate groups on plasmids (P) (A/P ratio) of 1.5 or more, plasmid migration from mitoNEET-$(KH)_9$ polyplexes was observed (Figure 1c). Meanwhile, no plasmid migration was detected in mitoNEET-$(RH)_9$ polyplexes even at an A/P ratio of 2.5. These results demonstrated a better stabilization by arginine residues than lysine ones through the enhanced ion-pairing between guanidine and phosphate hydrogen bonding.[16] The cationic sequence further influenced cytotoxicity to HeLa cells. After 24 h from polyplex treatment, mitoNEET-$(RH)_9$ polyplexes at an N/P ratio of 1.5 or 2 did not demonstrate considerable cytotoxicity. In contrast, those prepared at an N/P ratio of 2.5 or more showed a significant decrease in cell viability (Figure 1d). In the case of mitoNEET-$(KH)_9$ polyplexes, the cell viability decreased even at a low N/P ratio. As the same amount of free peptide showed higher cytotoxicity than polyplex formation (Figure S2a, Supporting Information), mitoNEET-$(KH)_9$ polyplexes with less structural robustness were possibly more toxic compared with mitoNEET-$(RH)_9$ ones. From these results, the N/P ratio of the polyplexes was set to 2 in the following experiments. Dose-responsive cytotoxicity analysis was conducted for mitoNEET-$(RH)_9$ polyplexes. Increasing the dose of polyplexes induced significant cytotoxicity, and polyplex treatment containing 1 μg or more plasmid was not safe for the cells under the experimental condition (initial cell number of 5000 cells on a 96-well plate) (Figure S2b, Supporting

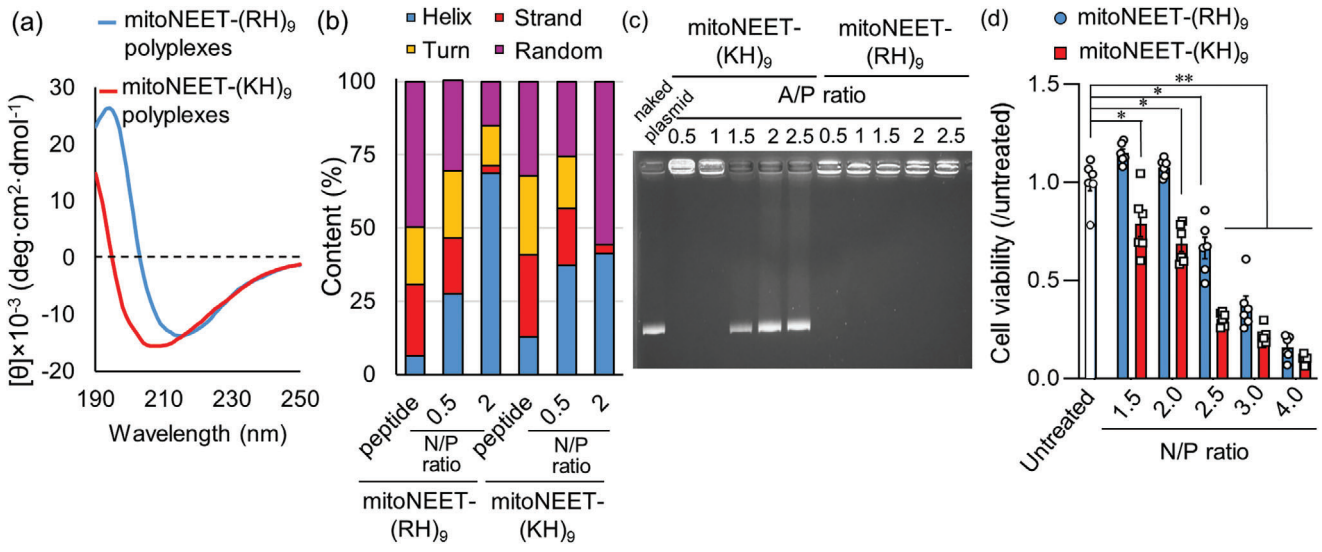

Figure 1. mitoNEET-$(RH)_9$ polyplexes exhibited better characteristics for mitochondrial gene delivery than mitoNEET-$(KH)_9$ polyplexes. a) CD spectrum of the polyplexes prepared from mitoNEET-$(RH)_9$ (Blue) and mitoNEET-$(KH)_9$ (Red) at an N/P ratio of 2. b) The content of the secondary structures of the peptide and polyplexes prepared at N/P ratio of 0.5 and 2. The contents were estimated from (a) and Figure S1 (Supporting Information). c) Tolerability of polyplexes at an N/P ratio of 2 against competitive polyanions at various A/P ratios. d) Cytotoxicity of the polyplexes at various N/P ratios to HeLa cells after 24 h of transfection. Biological replicates (n) = 6. Data represents the mean ± SEM. Each symbol in (d) represents biological replicates. *$p < 0.05$ and **$p < 0.01$ (one-way ANOVA with Dunnett's post hoc test compared with the untreated group for (d)).

Information). Based on these results, we treated the cells with the polyplex solution in the non-toxic condition in the following experiments.

2.2. mitoNEET-$(RH)_9$ Polyplexes Successfully Delivered Loaded Plasmids into the Mitochondria

We studied the mitochondria-targeting efficiency of the mitoNEET sequence by observing the intracellular trafficking behavior of Cy3-labeled plasmid encapsulated in polyplexes. Prior to the observation of intracellular distribution, we evaluated the cellular uptake efficiency of mitoNEET-$(RH)_9$ and -$(KH)_9$ polyplexes. The mitoNEET-$(RH)_9$ polyplexes showed a bit, but significant, higher uptake efficiency compared with mitoNEET-$(KH)_9$ ones (Figure S3a, Supporting Information), probably due to the higher stability of mitoNEET-$(RH)_9$. The less stable mitoNEET-$(KH)_9$ polyplexes might dissociated before cell entry. As their cellular uptake was inhibited by chlorpromazine (Figure S3b, Supporting Information), an inhibitor for clathrin- and caveolae-mediated endocytosis, the developed polyplexes entered through the endocytosis pathways. Then, we observed the intracellular distribution of the Cy3-labeled plasmid using confocal laser scanning microscopy (CLSM). In the CLSM images, the green, red, and blue pixels correspond to Cy3-labeled plasmid, mitochondria, and late endosomes/lysosomes. The yellow and cyan pixels represent Cy3-labeled plasmids in the mitochondria and late endosomes/lysosomes, respectively. After 3 h of polyplex treatment, most red pixels were co-localized with the blue pixels (**Figure 2**a,b; Figure S4a,b, Supporting Information), indicating that the polyplexes entered the cells through endocytosis. After an additional 3 h incubation, approximately half of the transfected polyplexes escaped from the endosomal compartments and successfully reached the mitochondria. The colocalization ratio after 24 h of transfection was similar to that after 6 h incubation, indicating that endosomal escape and translocation to the mitochondria occurred within 6 h. The orthogonal view of CLSM images demonstrated overlapping of green and red signals, indicating that the polyplexes entered inside the mitochondria (Figure S4c, Supporting Information). The contribution of the mitoNEET sequence and the α-helical structure for mitochondria-targeting was evaluated through CLSM observation of the following control polyplexes: mitoNEET-$(KH)_9$ polyplexes and non-mitochondria-targeting polyplexes composed of a cell-penetrating sequence (Tat: RKKRRQRRR)[17] fused with nine arginine-histidine repeats (Tat-$(RH)_9$) as a control peptide providing nuclear-specific gene expression (Figure S5a, Supporting Information). The polyplexes prepared from Tat-$(RH)_9$ showed similar endosomal escape ability derived from histidine residues to the mitoNEET-$(RH)_9$ ones, but obviously lower accumulation in the mitochondria than mitoNEET-$(RH)_9$ ones (Figure 2c; Figure S5b,c, Supporting Information), strongly indicating that the mitoNEET sequence helped to guide encapsulated plasmids to the mitochondria. Moreover, mitoNEET-$(KH)_9$ exhibited poor mitochondria-targeting efficiency compared with mitoNEET-$(RH)_9$ despite having the same MTS sequence. The difference in the co-localization ratio between mitoNEET-$(RH)_9$ and mitoNEET-$(KH)_9$ supported the idea that the secondary structure of the MTS, as shown in the results of CD spectroscopy (Figure 1a,b), was an important parameter for mitochondrial gene delivery. The higher cytotoxicity of mitoNEET-$(KH)_9$ polyplexes than mitoNEET-$(RH)_9$ ones might also affect the poor mitochondria-targeting efficiency of mitoNEET-$(KH)_9$ polyplexes.

Next, we investigated the molecular recognition mechanism of the mitoNEET-$(RH)_9$ polyplexes for mitochondrial uptake. Mitochondria have some import pathways for protein uptake (Figure S6a, Supporting Information). The mitoNEET protein can be recognized by the translocase of the mitochondrial outer membrane (TOM) 70 complexes, followed by being put in the membrane.[10] Then, polyplex accumulation in the mitochondria was evaluated after silencing TOM70 components using small interfering RNA (siRNA). As a control target, we selected TOM20 complexes, the most common pathway recognizing precursors of the mitochondrial matrix and intermembrane proteins.[18] The gene silencing efficiencies of the siRNAs designed according to previous reports[19] were respectively 51% for TOM20 and 63% for TOM70, evaluated by quantitative real-time PCR (qRT–PCR) analysis (Figure S6b, Supporting Information). The siRNA treatment did not induce considerable cytotoxicity (Figure S6c, Supporting Information), even after polyplex treatment. In contrast, TOM20 and TOM70 gene silencing decreased the mitochondrial membrane potential (Figure S6d, Supporting Information), an indicator of mitochondrial healthiness. However, TOM70 gene silencing only led to the limited accumulation of mitoNEET-$(RH)_9$ polyplexes in the mitochondria at 6 h of transfection, while TOM20 and scramble siRNA treatment did not affect it (Figure 2d; Figure S7a,b, Supporting Information). Further incubation of the cells did not improve the mitochondria-targeting efficiency. These results suggested that the mitoNEET sequence, even after polyplex formation, was recognized by TOM70 complexes and helped polyplexes enter the mitochondria.

The time-lapse observation captured the polyplex internalization into the mitochondria using super-resolution confocal microscopy. These confocal images clearly showed the uptake process of a polyplex to a mitochondrion (Figure 2e), which was the first demonstration of capturing the mitochondrial uptake of a nanoparticle. To further investigate the location of polyplexes, we employed correlative light and electron microscopy (CLEM)[20] and immunofluorescence staining of TFAM, a matrix protein for mitochondrial transcription. The merged images of CLEM observation demonstrated that the Cy5-labeled plasmid (green signal), which was co-localized with the red signals (mitochondria) in CLSM images, overlapped with the mitochondria as indicated by white arrows (Figure 2f; Figure S8, Supporting Information). Other green signals, indicated by arrowheads, did not overlap with the mitochondria in both the CLSM and CLEM images. Immunofluorescence staining of the mitochondrial matrix protein TFAM also demonstrated the co-localization of delivered plasmid (green signal) with TFAM (red signal) (Figure 2g; Figure S9a,c, Supporting Information), indicating the successful internalization of the plasmid into the mitochondria. We further immuno-stained TOM20 and evaluated the co-localization ratio of the plasmid and the mitochondrial outer membrane protein TOM20. The cyan signals representing TOM20 were located in the peripheral mitochondria (red pixels; Figure S9b, Supporting Information). Some green signals from Cy5-labeled plasmid were co-localized with the red pixels (mitochondria), but few were overlapped with cyan pixels (TOM20) (Figure S9d,Supporting

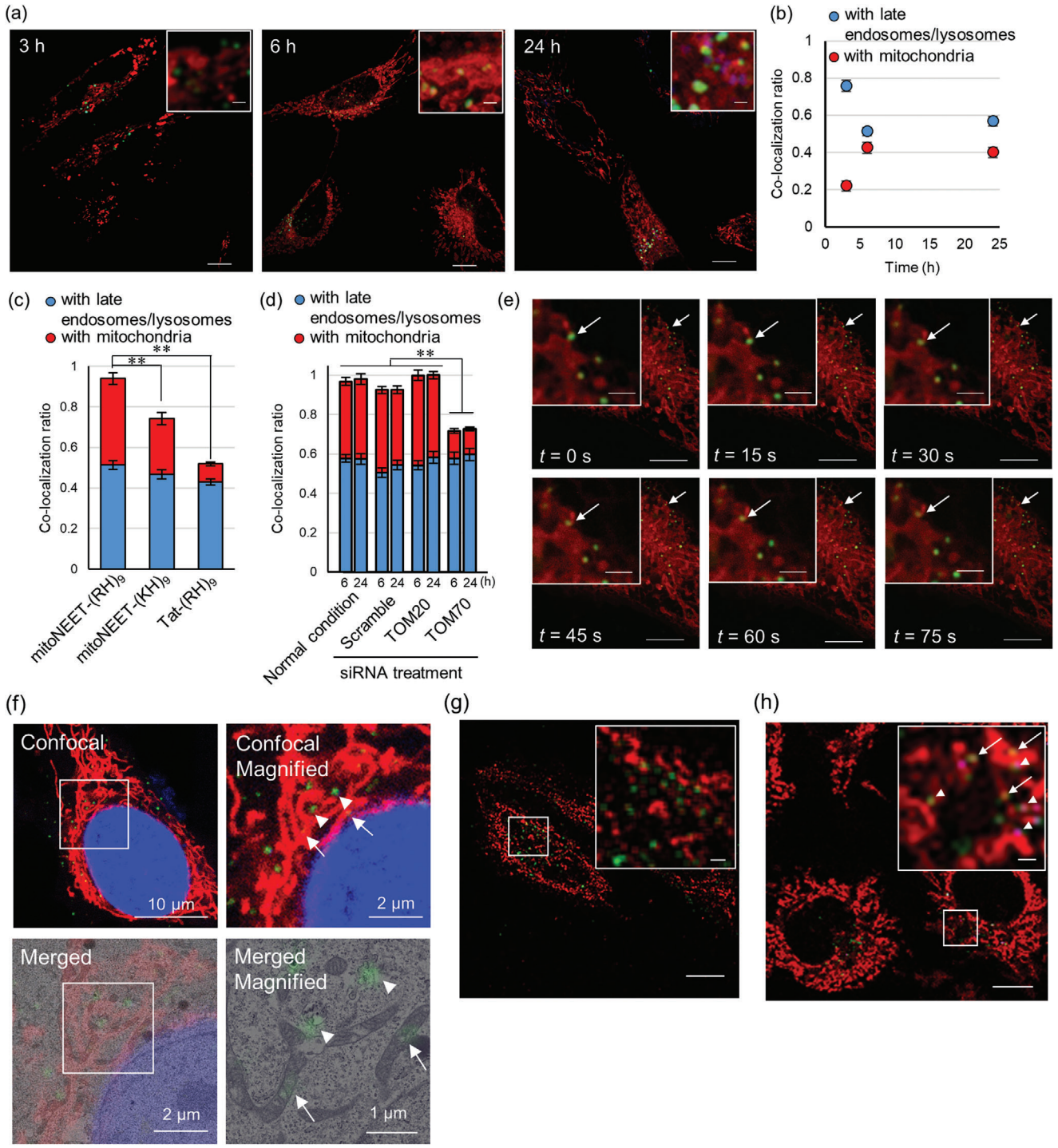

Figure 2. Internalization of plasmid loaded with mitoNEET-$(RH)_9$ polyplexes co-localized with the mitochondria. a) Representative CLSM images of the mitoNEET-$(RH)_9$ polyplexes after 3, 6, and 24 h of transfection. Red: mitochondria (MitoVIEW405), green: Cy3-labeled plasmids, and blue: late endosomes/lysosomes (LysoTracker Deep Red). b) Co-localization ratio of Cy3-labeled plasmid encapsulated in the mitoNEET-$(RH)_9$ polyplexes with the mitochondria (red) and late endosomes/lysosomes (blue) calculated from 35 individual cells. c,d) Comparing the co-localization ratios of Cy3-loaded plasmid (c) encapsulated in the mitoNEET-$(RH)_9$, -$(KH)_9$, and Tat-$(RH)_9$ polyplexes and (d) after siRNA treatment targeting TOM20 and TOM70 with the mitochondria (red) and late endosomes/lysosomes (blue) after 6 h of transfection. The co-localization ratios were calculated from 35 individual cells. The values of mitoNEET-$(RH)_9$ polyplexes in (c) were the same as those in (b) after 6 h of transfection. e) Superresolution microscopy of mitochondrial uptake. Red: Mitochondria (MitoBright deep red) and Green: Cy3-labeled plasmids. White arrows indicate the uptake behavior of Cy3-labeled plasmid. f) CLEM images of HeLa cells after mitoNEET-$(RH)_9$ polyplex treatment. Red: Mitochondria (MitoTracker red CMXRos) and Green: Cy5-labeled plasmids. Arrows and arrowheads represent the Cy5 signal inside or outside of the mitochondria, respectively. g) Immunofluorescence staining of TFAM after 24 h

Information). Note that, the co-localization ratio of the Cy5-plasmid with TFAM was 8.1 ± 1.5% (Figure S9c, Supporting Information), lower than that with mitochondria (16.7 ± 2.4%) in Figure S9d (Supporting Information). These results suggested that a part of polyplexes reaching the mitochondria entered the mitochondrial matrix. The results of the CLEM observation and immunofluorescence staining strongly indicated the secured mitochondrial uptake of mitoNEET-$(RH)_9$ polyplexes.

The release of the loaded plasmid from the polyplexes in the mitochondria was evaluated by monitoring Förster resonance energy transfer (FRET) signals of Cy3/Cy5 double-labeled plasmid.[21] An encapsulation of the Cy3/Cy5 double-labeled plasmid in the polyplexes increased the FRET signal compared with the naked state (Figure S10a, Supporting Information). Thus, as FRET signal can be reduced by the release of plasmid from polyplexes, monitoring the reduction of intracellular FRET signal enables us to examine the plasmid release inside the cells. The CLSM images showed that some FRET signals disappeared inside the mitochondria while maintained outside (Figure 2h; Figure S10b–d, Supporting Information), indicating that the plasmid was condensed in the polyplexes before mitochondrial uptake and released inside the mitochondria or during the uptake process. Note that, the Cy5 signals were derived from FRET, as Cy5 single-labeled plasmid was excited by a 633 nm laser but not by a 488 nm laser (Figure S10e, Supporting Information).

2.3. mitoNEET-$(RH)_9$ Polyplexes Led to Mitochondria-Specific Gene Expression

To evaluate exogenous gene expression in the mitochondria, we prepared a plasmid encoding GFP with a mitochondria-specific promoter (yeast cytochrome c oxidase subunit II promoter) based on our previous findings.[22] The promoter from the yeast mtDNA is known to work in the mitochondria of other organisms including mammalian cells.[23] The mitochondrial codon was used in the GFP-encoding region to ensure GFP expression only in the mitochondria. The TGG codon at amino acid 58 (tryptophan, bases: 172–174) in the conventional GFP sequence was replaced with TGA, which encodes tryptophan in the mitochondria codon but is a nuclear stop codon (Figure S11a, Supporting Information; top). As a control plasmid, the CGC codon in GFP (amino acid 74, arginine, bases: 220–222) was replaced with AGA, a stop codon in the mitochondria but encoding arginine in the nuclear codon (Figure S11a, Supporting Information; bottom). The plasmids expressing GFP in the mitochondria and cell nuclei were denoted by pmtGFP and pnuclearGFP, respectively. We transfected the polyplexes loaded with each plasmid into HeLa cells. The pmtGFP-loading mitoNEET-$(RH)_9$ polyplexes showed bright green signals in the CLSM images, while pnuclearGFP did not (**Figure 3**a; Figure S12a, Supporting Information), indicating that the delivered pmtGFP expressed in the mitochondria. Flow cytometry analysis revealed a solid GFP expression from the mitoNEET-$(RH)_9$ polyplexes while Tat-$(RH)_9$ ones provided negligible expression (Figure 3b). The GFP intensity from mitoNEET-$(RH)_9$ polyplexes reached a maximum after 24 h of transfection, and decreased after 72 h (Figure 3c; Figure S12b, Supporting Information), which indicated the transient gene expression in the mitochondria. Quantification of the amount of transfected plasmid showed a rapid decrement of plasmids normalized by β-actin genes in the cells (Figure S13, Supporting Information), which could result in transient gene expression. Gene silencing of TOM70 complexes dramatically decreased GFP expression at various time points, while control gene silencing targeting TOM20 complexes and scramble siRNA treatment did not affect (Figure 3d,e; Figure S12c, Supporting Information). These results, consistent with the uptake experiments (Figure 2d), confirmed the responsibility of TOM70 complexes for polyplex entry. Note that, expressed GFP was less co-localized with the mitochondria after TOM20 and TOM70 gene silencing (Figure S12d, Supporting Information), possibly due to the upregulation of the mitochondrial quality control system caused by a decrease of mitochondrial membrane potential.[24]

In CLSM images, although GFP expression was obtained inside the mitochondria, some green signals were observed outside the mitochondria, indicating that the expressed GFP was released from the mitochondria. We then evaluated the location of the expressed GFP to understand this phenomenon. Mitochondria have quality control mechanisms for the steady-state turnover of mitochondrial proteins,[25] finally delivering their contents to lysosomes for degradation. Thus, we examined the colocalization ratio between the GFP and lysosomes. At 6 h of transfection, although the GFP intensity was weak, most GFP signals (green pixels) overlapped with the mitochondria (red pixels) (Figure 3f,g; Figure S14, Supporting Information). Further incubation of the cells demonstrated an increase in the colocalization ratio of GFP with late endosomes/ lysosomes (blue pixels) and a decrease with mitochondria. These colocalization ratios reached a plateau after 24 h of transfection, probably due to the balance between the expression and release speed of GFP in the mitochondria. The transportation of GFP to lysosomes may induce the degradation of GFP, resulting in decreased fluorescence intensity (Figure 3c).

2.4. mitoNEET-$(RH)_9$ Polyplexes Restored mtDNA-Depleted Cells by Multiple Gene Expressions from Exogenous mtDNA

As a model experiment to engineer the mitochondria, we aimed to restore the mitochondrial function of mtDNA-depleted HeLa cells (HeLa-ρ° cells). For mtDNA preparation, mtDNA was extracted from a normal cell line (HEK293 cell), not HeLa cell, to avoid the risk of contaminating mutated mtDNA in the cancer cells.[26] An OriC cassette was inserted into the extracted mtDNA for in vitro amplification by the replication cycle reaction (Figure S11b,c, Supporting Information).[27] DLS measurements showed a slightly larger cumulant diameter of mtDNA-

of mitoNEET-$(RH)_9$ polyplex treatment. Red: TFAM and green: Cy5-labeled plasmids. h) Estimation of the polyplex dissociation by observing FRET signals from Cy3/Cy5-labeled plasmid. Arrows and arrowheads represent the Cy5 signal without or with co-localizing with the Cy3 signal, respectively. Red: Mitochondria (MitoTracker red CMXRos), green: Cy3, and magenta: Cy5. Scale bar, 10 μm in the whole image and 1 μm in the magnified image in (a), (g), and (h). Data represents the mean ± SEM. $^{**}p < 0.01$ (one-way ANOVA followed by Tukey's post hoc test for (c) and by Dunnett's post hoc test compared with the normal condition group for (d)).

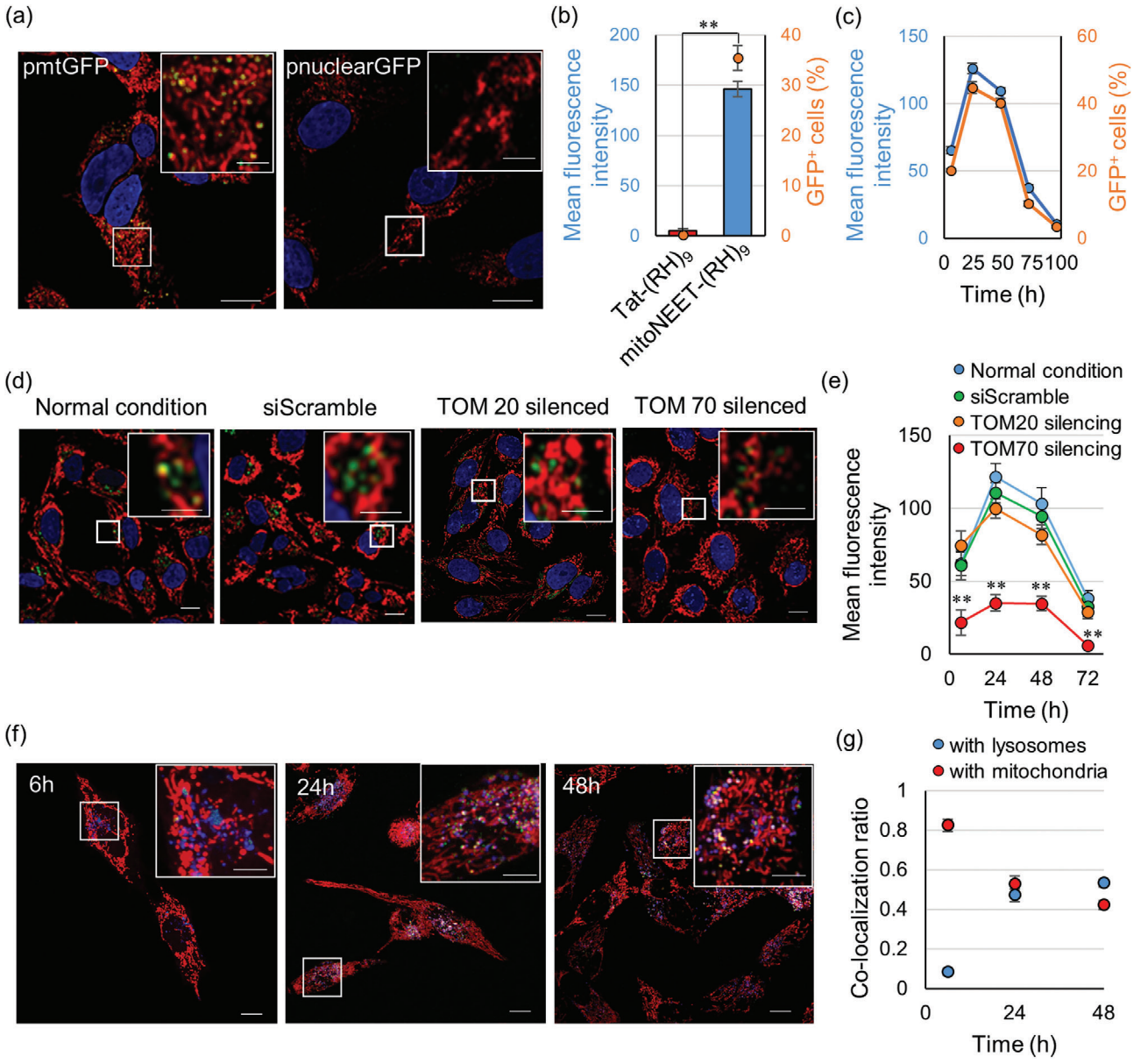

Figure 3. mitoNEET-$(RH)_9$ polyplexes efficiently expressed GFP in the mitochondria of the HeLa cells. a) Representative CLSM images of GFP expression from constructed plasmids. Red: mitochondria (MitoTracker Red CMXRos), green: GFP, and blue: nuclei (Hoechst33342). b) Comparing GFP expression of mitoNEET-$(RH)_9$ polyplexes with that of Tat-$(RH)_9$ polyplexes. Bar: Mean fluorescence intensity (left Y axis) and Dot: the percentage of GFP^+ cells (right Y axis). Biological replicates (n) = 4. c) Time-course of GFP expression analyzed by flow cytometry. Blue: Mean fluorescence intensity (left Y axis); Orange: The percentage of GFP^+ cells (right Y axis). Biological replicates (n) = 4. d) Representative CLSM images of transfected cells after siRNA treatment. Red: mitochondria (MitoTracker Red CMXRos), green: GFP, and blue: nuclei (Hoechst 33342). e) Flow cytometry analysis of GFP expression after gene silencing of TOM20 and TOM70 at various time points. Bar: Mean fluorescence intensity (left Y axis) and Dot: the percentage of GFP^+ cells (right Y axis). Biological replicates (n) = 4. f) Representative CLSM images of transfected cells at various time points. Red: mitochondria (MitoTracker Red CMXRos), green: GFP, and blue: late endosomes and lysosomes (LysoTracker Deep red). g) Co-localization ratios of GFP with the mitochondria and lysosomes were calculated from 35 individual cells. Scale bar, 10 μm in the whole images and 5 μm in the magnified images. Data represent the mean ± SEM. $^{**}p < 0.01$ (unpaired 2-tailed Student's t-test for (b) and one-way ANOVA with Dunnett's post hoc test compared with the normal condition group for (e)).

loading polyplexes and similar PDI and ζ-potential values to pmtGFP-loading polyplexes (155 ± 6.3 nm for size, 0.22 ± 0.01 for PDI, and 16.2 ± 0.3 mV for ζ-potential), probably because mtDNA (16.7 kbp) is larger than pmtGFP (5.1 kbp). The mtDNA-loading polyplex characteristics were also evaluated through CD measurement and structural stability assay. The secondary structure and stability of mtDNA-loading polyplexes were similar to those with pmtGFP (Figure S15a–c, Supporting Information), indicating that the mitoNEET-$(RH)_9$ polyplexes effectively work to deliver DNA molecules with relatively large size. Cytotoxicity

assay of mitoNEET-$(RH)_9$ polyplexes with mtDNA demonstrated that polyplex treatment containing 1 μg or more plasmid induced considerable cytotoxicity to the HeLa-ρ° cells under the experimental condition (initial cell number of 5000 cells on a 96-well plate) (Figure S15d, Supporting Information). These results led us to treat the cells with the polyplex solution in a nontoxic condition in the following experiments. Then, we evaluated the targeting efficiency of the mitoNEET sequence to HeLa-ρ° cells because the decrease of the mitochondrial membrane potential in ρ° cells due to the lack of mtDNA may reduce the mitochondria-targeting efficiency. The mitochondrial membrane potential in the HeLa-ρ° cells was different from those in the wild-type (WT) HeLa cells (Figure S16a, Supporting Information), but mitoNEET-$(RH)_9$ polyplexes successfully guided the loaded plasmid to the mitochondria (Figure S16b,d, Supporting Information). mtDNA-loading polyplexes were also co-localized with the mitochondria (Figure S16b–d, Supporting Information), suggesting that mitoNEET-$(RH)_9$ polyplexes can successfully guide the loaded DNA with at least within 16.7 kbp to the mitochondria in HeLa-ρ° cells.

The expression of mtDNA in HeLa-ρ° cells was examined via qRT–PCR. The exogenous mtDNA transfection performed 353- and 42-fold higher levels of all encoded genes in mtDNA except *cytochrome b* (*Cyt b*) gene than in untreated HeLa-ρ° cells (**Figure 4**a). The solid expression from exogenous mtDNA allowed us to expect the recovery of mitochondrial functions in HeLa-ρ° cells. Noteworthy, the OriC sequence affected the mtDNA expression; the OriC insertion lacked Cyt b expression and slightly prevented the expression of *ND4*, *ND5*, and *ND6* close to the cassette, but the expression of other genes located far from the OriC was not inhibited. Also, there was still a significant difference in the mtDNA expression levels between mtDNA-transfected HeLa-ρ° cells and WT-HeLa cells. We performed immunofluorescence imaging after mtDNA transfection to examine the exogenous mtDNA expression at the protein level. As representative proteins with high and low transcript levels, ND1 and Cyt b were selected, respectively. Green signals representing immunofluorescence stained ND1 and Cyt b were observed in WT-HeLa cells, but not in the untreated HeLa-ρ° cells due to the lack of mtDNA (Figure 4b). After exogenous mtDNA transfection to the HeLa-ρ° cells, green signals from only ND1 were detected. Quantification of green signal levels from CLSM images revealed that exogenous mtDNA provided significant ND1 expression but not Cyt b (Figure 4c), which was consistent with the transcript levels.

Next, we assessed the mitochondrial functions of HeLa-ρ° cells after mtDNA transfection. HeLa-ρ° cells cannot survive without highly concentrated pyruvate and uridine as supplements due to the lack of mtDNA.[28] Thus, we demonstrated the improvement of mitochondrial functions by mtDNA under the low supplementation levels, where HeLa-ρ° cells can grow only when exogenous mtDNA recovered its mitochondrial functions. We measured the NAD^+/NADH ratio in HeLa-ρ° cells, a commonly employed parameter to evaluate the mitochondrial complex I activity.[29] The NAD^+/NADH ratio after 2 days from mtDNA transfection was significantly higher than that of the untreated and pmtGFP-treated HeLa-ρ° cells (Figure 4d). Triple mtDNA transfection further improved the ratio after 6 days from the first transfection, suggesting that exogenous mtDNA improved the mitochondrial complex I activity. the NAD^+/NADH ratio after triple mtDNA transfection did not reach that of the WT HeLa cells. The oxygen consumption rate (OCR) and extracellular acidification rate (ECAR) of the HeLa-ρ° cells were then measured using a flux analyzer to evaluate the energy production after mtDNA transfection. OCR and ECAR are correlated with mitochondrial respiration and glycolysis, respectively. The triple mtDNA transfection significantly upregulated both OCR and ECAR in the HeLa-ρ° cells after 7 days of the first transfection compared with the untreated group, although the improvement of OCR was limited (Figure 4e,f). The enhanced energy production by mtDNA transfection expected us to improve the cell viability of HeLa-ρ° cells. As the CCK-8 assay kit can react with the electrons generated from NADH to NAD^+ conversion, this assay should correlate with the mitochondrial activity. By CCK-8 assay, the cell viability of the mtDNA-transfected HeLa-ρ° cells was higher than that of untreated groups 11 days after transfection (Figure S17, Supporting Information). The triple mtDNA transfection further enhanced cell viability. As pmtGFP transfection did not improve the cell viability even after triple transfections, it was reasonable that transfected mtDNA contributed to cell proliferation. Note that, the improvement of cell viability was transient. The quantification of mtDNA revealed that the exogenous mtDNA was gradually degraded in the HeLa-ρ° cells (Figure S18, Supporting Information), suggesting that the transfected mtDNA was not fixed in the ρ° cells.

Mitochondrial morphology represents key aspects of mitochondrial and cellular health.[30] In particular, elongated and branched mitochondria, which are determined by measuring aspect ratio (AR; the ratio of the major and minor axes) and form factor (FF; $(\text{Perimeter})^2/4\pi(\text{Area})$), are associated with high mitochondrial respiration activity.[31] Thus, these values in the HeLa-ρ° cells were measured from confocal images (**Figure 5**a). The mtDNA transfection, consistent with the NAD^+/NADH ratio and OCR measurements (Figure 4b–d), significantly increased both AR and FF in the HeLa-ρ° cells (Figure 5b,c). Intriguingly, pmtGFP transfection also slightly improved AR and FF. However, as mtDNA transfection was more critical than pmtGFP for the morphological changes, exogenous mtDNA significantly contributed to improving mitochondrial conditions.

3. Discussion

Approaches to engineering the mitochondrial genome are attractive for disease treatment and fundamental research on mitochondria. The major challenge is securing mitochondrial gene expression. Allotopic delivery strategies expressing MTS-fused proteins in the cell nuclei are mainstream in mitochondrial gene therapy.[32] However, the limited performance of allotopic expression due to the two modes of transportation may restrict its application.[33] Thus, the direct gene delivery into the mitochondria is promising for providing functional proteins with the mitochondria. Classically, lipophilic cations, such as triphenylphosphine, have been used as a mitochondria-targeting module[8] because the cationic charge facilitates the electrostatic interaction with the highly negatively charged mitochondrial membrane. However, lipophilic cations also accelerate the interaction with other negatively charged biomacromolecules, ultimately leading to unfavorable cytotoxicity and limited applications.[34] The

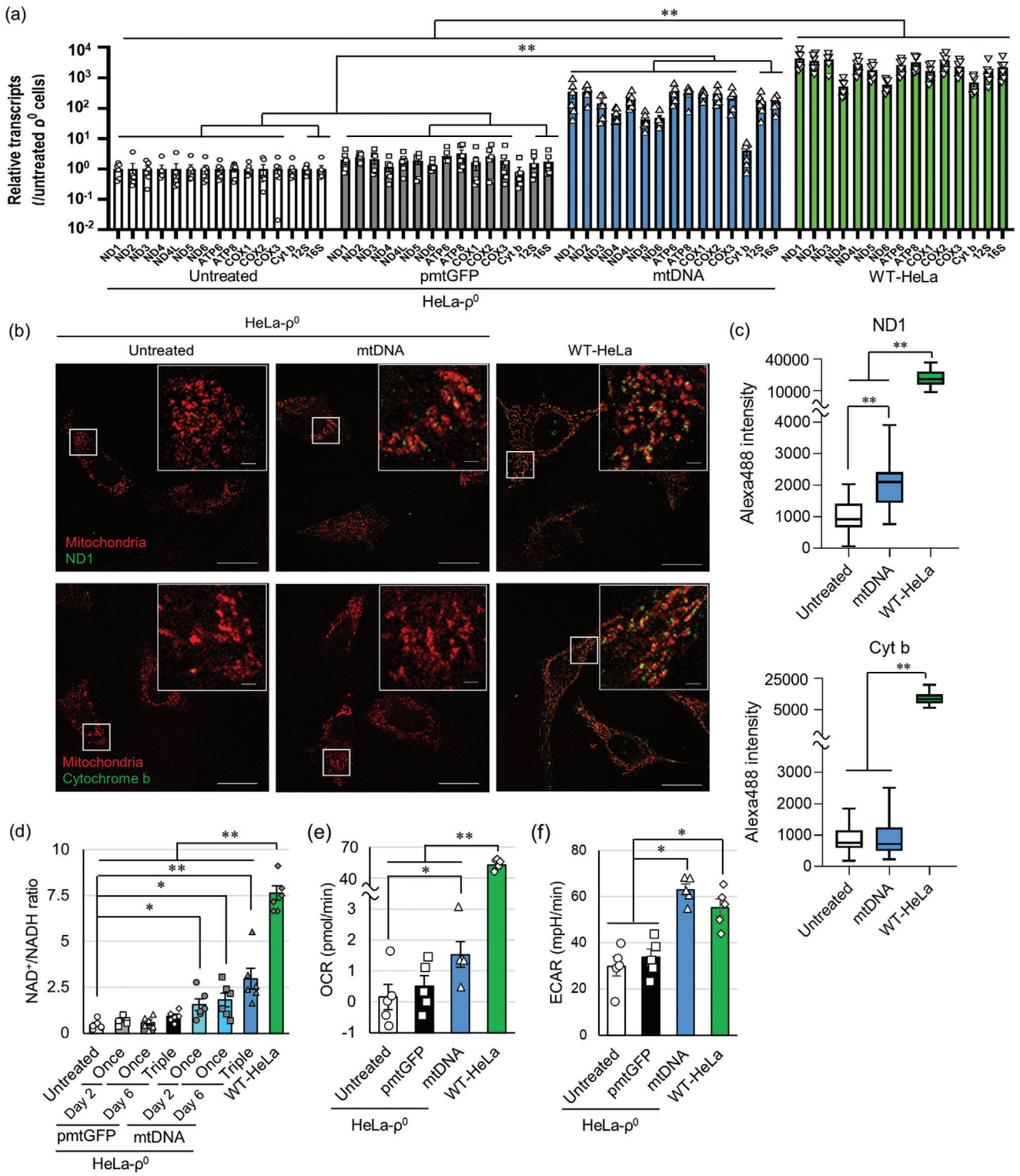

Figure 4. Mitochondrial function was restored by multiple exogenous mtDNA expressions in the HeLa-ρ° cell line. a) Mitochondrial RNA abundance quantified by qRT-PCR analysis. Biological replicates (n) = 6. b) Representative CLSM images of ND1 and Cyt b immunofluorescence staining. Red: Mitochondria (MitoTracker red CMXRos) and green: ND1 or Cyt b. Scale bar, 10 µm in the whole images and 1 µm in the magnified images. c) Boxplot representation of the ND1 and Cyt b intensities in the cells. The boxes and lines in the boxes represent the interquartile range and the median, respectively. The upper and lower whiskers represent the highest and lowest values. The intensities were calculated from 20 individual cells. d) NAD^+/NADH assay after transfection. Biological replicates (n) = 6. e) OCR and f) ECAR values of HeLa-ρ° cells. Biological replicates (n) = 5. Scale bar, 5 µm. Data represent the mean ± SEM. Each dot represents biological repeats. $^*p < 0.05$ and $^{**}p < 0.01$ (one-way ANOVA followed by Tukey's post hoc test for (a), (c), and Dunnett's post hoc test compared with the untreated group for d–f)).

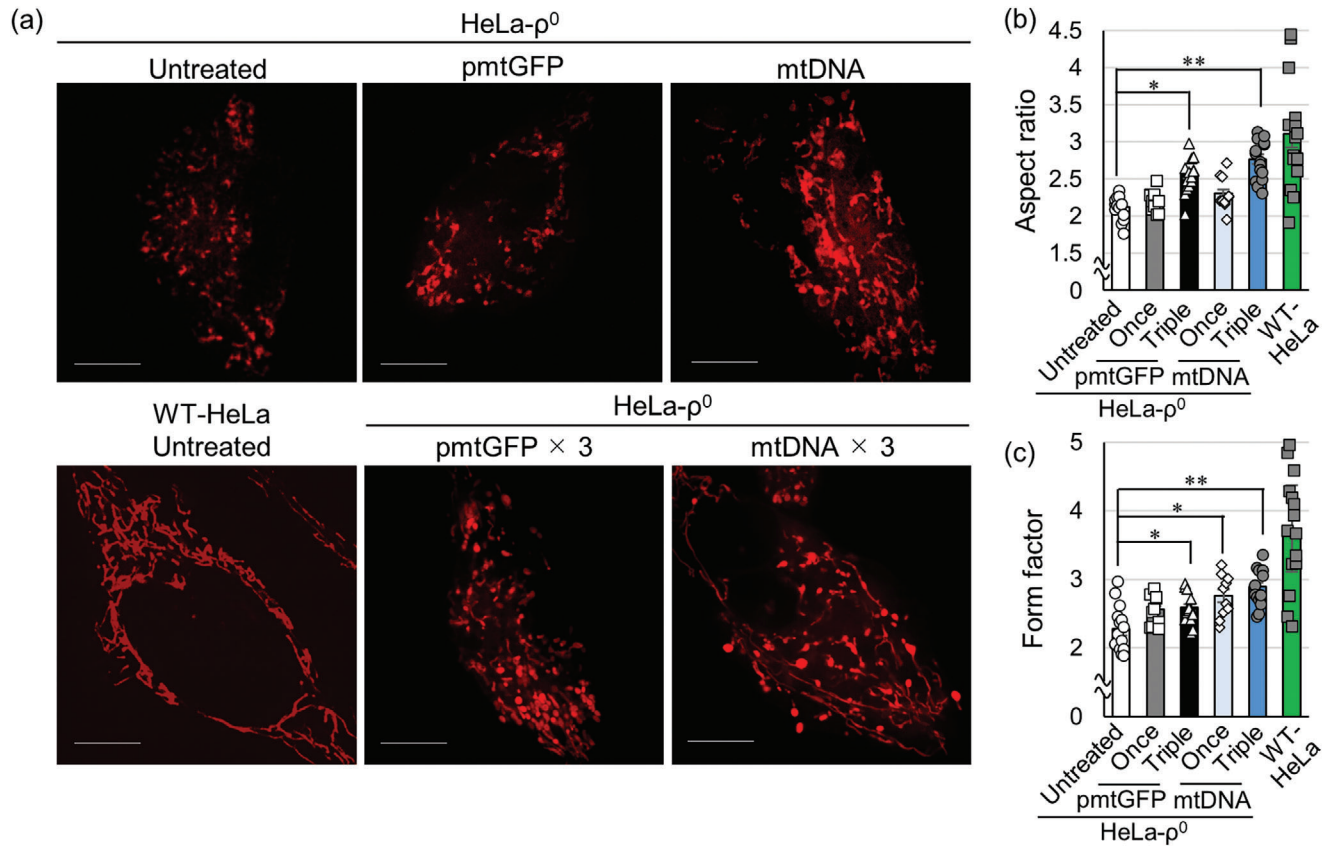

Figure 5. Morphological changes of the mitochondria after mtDNA transfection. a) Representative CLSM images of HeLa-ρ° cells stained by MitoTracker red CMXRos after mtDNA transfection. Morphological parameters of the mitochondria calculated from CLSM images; b) aspect ratio and c) form factor. These parameters were calculated from 15 individual cells for the triple transfection and the untreated groups and 10 individual cells for the single transfection groups. Scale bar, 5 μm. Data represent the mean ± SEM. Each dot represents biological repeats. $*p < 0.05$ and $**p < 0.01$ (one-way ANOVA with Dunnett's post hoc test compared with the untreated group for (b-c)).

use of MTS is a promising way to integrate a mitochondria-targeting function into delivery carriers with minimal cytotoxicity, but the transfection efficiency is insufficient.[8] To determine why MTS-based carriers have low efficiency, we focused on the import pathway of the MTSs used in previous reports. The previously reported MTSs were designed from mitochondrial intermembrane or matrix proteins imported through the presequence pathway mediated by TOM20.[18a,35] The mitochondrial proteins recognized by the TOM20 complexes were then transferred to the mitochondrial intermembrane space through the barrel-like TOM40 complexes (Figure S8a, Supporting Information).[18] However, as the ordinary TOM20-TOM40 route opens for proteins with up to 2.2 nm,[36] it could be inappropriate for the transportation of submicron-sized nanoparticles.

Thus, this study focused on another import machinery mediated by TOM70, which directly recruits transmembrane proteins to the outer membrane independently of the TOM40-mediated pathway.[13,37] The N-terminal signal domain of mitoNEET protein, which can be recruited via TOM70 recognition, was used as an MTS, followed by fusing a cationic segment $(RH)_9$. The designed mitoNEET-$(RH)_9$ polyplexes resulted in the mitochondrial accumulation of the loaded plasmid and gene expression (Figures 2a and 3a–c) by providing polyplexes with structural robustness and an α-helical mitochondria-targeting structure with minimal cytotoxicity (Figure 1). Surprisingly, the arginine repeat in the cationic segment contributed to better polyplex cytotoxicity, stability, and secondary structure for mitochondrial gene expression than the lysine repeat, although the mitoNEET sequence was common. Gene silencing of TOM70 reduced the mitochondrial accumulation of polyplexes (Figures 2c,d and 3d,e), indicating that TOM70 played a key role as a signpost for the mitoNEET sequence to guide polyplexes to the mitochondria. Moreover, the detailed analysis of the intracellular trafficking behavior of the mitoNEET-$(RH)_9$ polyplexes revealed an intriguing and ambiguous phenomenon, the uptake mechanism into the mitochondria. The super-resolution microscopic observation captured the mitochondrial uptake of the polyplexes (Figure 2e). As the FRET observation in Figure 2h demonstrated the polyplex formation before mitochondrial entry, the polyplexes could be ingested with keeping its structure. Furthermore, the CLEM observation and immunofluorescence staining of TFAM and TOM20 revealed that the loaded plasmids were co-localized with inside the mitochondria (Figure 2f,g; Figure S9, Supporting Information), strongly suggesting the entry of the loaded plasmids into the mitochondria. Meanwhile, the mitochondrial uptake mechanism of large molecules, including polyplexes, is still unclear. As

alternative transport pathways to translocase channels for large molecules, such as lysosome-like organelle, have been suggested for mitochondrial quality control,[38] the mitoNEET-$(RH)_9$ polyplexes might be digested by the mitochondria through these alternative pathways after recognition by TOM70. The internalization of polyplexes into the mitochondria without dissociation confirmed that the loaded plasmid was successfully transported without enzymatic degradation, although plasmids possess less tolerability in the cytosol.[39] This phenomenon may encourage further evaluation of mitochondrial uptake toward exogenous macromolecules. After mitochondrial uptake, the positively charged polyplexes might be drawn to the inner membrane with a large negative potential through electrostatic interactions, which could lead to the further internalization of polyplexes into the matrix for gene expression. FRET observation in Figure 2h demonstrated the release of the loaded plasmid inside the mitochondria, probably due to polyion exchange reactions against charged mitochondrial macromolecules, such as proteins and nucleic acids. The efficient release of the loaded plasmid may lead to the smooth transition of the plasmid to the mitochondrial transcriptional pathway. The time-lapse imaging of FRET signals could provide insights into when polyplexes dissociate during the mitochondrial uptake process and how polyplexes traffic in the mitochondria. While mitochondria-specific gene expression was obtained (Figure 3a–c), the detailed mechanism of mitochondrial transcription and translation of exogenous genes remains unexplored. The current system indeed provided transient gene expression due to the degradation of transfected plasmids (Figure S13, Supporting Information). Methylated bases in exogenous DNA, which correlate with the copy number and gene expression efficiency,[40] could affect the stability of plasmids in the mitochondria. Determining a mitochondrial gene expression mechanism of exogenous genes could improve mitochondrial gene delivery efficiency, such as prolonged gene expression.

The most highlighted outcome in this study is the improvement of HeLa-ρ° cells by simultaneous gene expression from the exogenous mtDNA. The mtDNA-loading polyplexes provided empty mitochondria in HeLa-ρ° cells with efficient, multiple gene expressions encoded in mtDNA (Figure 4a–c), demonstrating that intact mtDNA was surely transfected into the mitochondria. The transfection efficiency was enough to improve mitochondrial function in HeLa-ρ° cells, resulting in enhanced mitochondrial functions, including the complex I activity and OCR (Figure 4d–f). This is the first demonstration of restoring ρ° cell lines lacking whole mtDNA. Surprisingly, ECAR correlated with glycolysis was also enhanced by mtDNA transfection. The increased ECAR indicated that more pyruvate reduction to lactate in glycolysis. In the ρ° cells lacking a complete electron transport chain and the tricarboxylic acid (TCA) cycle, the NAD^+ produced by NADH oxidation at mitochondrial complex I activated by mtDNA introduction might be partially used for TCA cycle but mainly consumed for cytosolic pyruvate reduction, finally inducing ECAR upregulation. The positive effect of mtDNA transfection was further observed in the mitochondrial morphology, which correlates with mitochondrial health.[30a] The mitochondria in the mtDNA-transfected cells, especially after triple transfection, formed a network structure with an increased AR and FF (Figure 5). Intriguingly, pmtGFP transfection also improved these values. Two possibilities could explain this phenomenon; introducing plasmids into empty mitochondria, even if they are decoy molecules, can affect mitochondrial morphology, and mitoNEET-$(RH)_9$ peptide itself affected it. However, mtDNA transfection demonstrated a more significant improvement, suggesting that the introduced mtDNA strongly contributed to improving the mitochondrial conditions with help in the transfection procedure. It should be noted that the improvement was transient, and transfected mtDNA was not fixed in the HeLa-ρ° cells (Figures S17 and S18, Supporting Information). Moreover, the OriC insertion, which was necessary for amplification, influenced the expression efficiency of the exogenous mtDNA (Figure 4a–c). The solid improvement was observed in the mitochondrial complex I activity after exogenous mtDNA transfection, but that in OCR was restrictive, although it was significant. The insufficient expression of cytochrome b due to the OriC insertion possibly caused the immature complex III formation, leading to unsatisfied electron transportation for energy production. These results demanded a need to refine the mtDNA design, as well as peptide design, to approach the native expression profile more closely.

Direct gene delivery to the mitochondria can be a more promising mitochondrial genome editing than allotopic expression. The current system completed inside the mitochondria can provide a variety of proteins, including genome editors, without any adverse effect on the nuclear genome. Indeed, mtDNA editing via allotopic expression causes severe off-target effects on the nuclear genome.[41] Moreover, multiple gene expression of functional proteins with a marker protein, such as GFP, enables us to identify the cells containing the engineered mitochondria. The lack of selective markers has impeded the development of mitochondrial genome engineering. To this issue, the mitoNEET-$(RH)_9$ polyplexes may provide innovation in both fundamental and applied research on mitochondria through the detailed analysis of the cells sorted by markers. The knock-in of homologous DNA is also an attractive application of mitoNEET-$(RH)_9$ polyplexes. As no DNA import machinery for mammalian mitochondria has been provided,[42] knocking-in donor DNA into mtDNA should be unattainable without using the effective mitochondrial gene delivery carriers in this study.

4. Conclusion

We have reported a versatile strategy to securely deliver DNA molecules into the mitochondria by using polyplexes composed of mitoNEET-$(RH)_9$ peptides, which accomplished sufficient multiple-gene expression to improve mitochondrial energy production in mtDNA-depleted ρ° cells. The molecular design of the peptide, including both the MTS and the cationic sequence, was a dominant factor in this successful mitochondrial gene delivery and can serve as a guiding principle for the development of other mitochondrial gene delivery carriers. The current multiple-gene expression system in each mitochondrion based on the mitoNEET-$(RH)_9$ peptide can overcome the limitation of previous techniques and thus contributes to further exploration of mitochondrial engineering technologies, such as single-mitochondrion analysis and clinical application to inherited mitochondrial diseases.

Supporting Information

Supporting Information is available from the Wiley Online Library or from the author.

Acknowledgements

This research was financially supported by Japan Science and Technology Agency Exploratory Research for Advanced Technology (JST-ERATO; K.N., Grant JPMJER1602), The Ministry of Education, Culture, Sports, Science and Technology (MEXT) Data Creation and Utilization-Type Material Research and Development Project (JPMXP1122714694 to K.N.), a Grant-in-Aid for Scientific Research (S) (23H05473; M.Y.), a Grant-in-Aid for Scientific Research (S) (22H04975; K.N.), a Grant-in-Aid for Research Activity Start-up (21K20523; N.Y.), and a Grant-in-Aid for Early Carrier Scientists (23K17217; N.Y.), JST-PRESTO (JPMJPR228A; N.Y.) and JST-CREST (JPMJCR18S6; M.S.). The authors thank M.G. for technical assistance.

Conflict of Interest

The authors declare no conflict of interest.

Data Availability Statement

The data that support the findings of this study are available in the supplementary material of this article.

Keywords

gene delivery, mitochondria, mitochondria-targeting peptide, polyplex

Received: May 30, 2023
Revised: September 26, 2023
Published online: November 1, 2023

[1] J. B. Spinelli, M. C. Haigis, *Nat. Cell Biol.* **2018**, *20*, 745.
[2] a) S. Anderson, A. T. Bankier, B. G. Barrell, M. H. L. De Bruijn, A. R. Coulson, J. Drouin, I. C. Eperon, D. P. Nierlich, B. A. Roe, F. Sanger, P. H. Schreier, A. J. H. Smith, R. Staden, I. G. Young, *Nature* **1981**, *290*, 457; b) S. Rath, R. Sharma, R. Gupta, T. Ast, C. Chan, T. J. Durham, R. P. Goodman, Z. Grabarek, M. E. Haas, W. H. W. Hung, P. R. Joshi, A. A. Jourdain, S. H. Kim, A. V. Kotrys, S. S. Lam, J. G. Mccoy, J. D. Meisel, M. Miranda, A. Panda, A. Patgiri, R. Rogers, S. Sadre, H. Shah, O. S. Skinner, T. L. To, M. A. Walker, H. Wang, P. S. Ward, J. Wengrod, C. C. Yuan, et al., *Nucleic Acids Res.* **2021**, *49*, D1541.
[3] a) J. B. Stewart, P. F. Chinnery, *Nat. Rev. Genet.* **2015**, *16*, 530; b) G. S. Gorman, P. F. Chinnery, S. Dimauro, M. Hirano, Y. Koga, R. Mcfarland, A. Suomalainen, D. R. Thorburn, M. Zeviani, D. M. Turnbull, *Nat. Rev. Dis. Primers* **2016**, *2*, 16080.
[4] a) N.-G. Larsson, *Annu. Rev. Biochem.* **2010**, *79*, 683; b) D. F. Bogenhagen, *Biochim. Biophys. Acta* **2012**, *1819*, 914.
[5] a) A. Ryzhkova, M. Sazonova, V. Sinyov, E. Galitsyna, M. A. Chicheva, A. Melnichenko, A. Grechko, A. Postnov, A. Orekhov, T. Shkurat, *Ther. Clin. Risk Manage.* **2018**, *2018*, 1933; b) S. Zapico, *Aging Dis.* **2013**, *4*, 364; c) R. W. Taylor, D. M. Turnbull, *Nat. Rev. Genet.* **2005**, *6*, 389.
[6] J. Nunnari, A. Suomalainen, *Cell* **2012**, *148*, 1145.
[7] T. Chen, J. He, Y. Huang, W. Zhao, *J. Human Gen.* **2011**, *56*, 689.
[8] a) Y. Yamada, Satrialdi, M. Hibino, D. Sasaki, J. Abe, H. Harashima, *Adv. Drug Delivery Rev.* **2020**, *154–155*, 187; b) N. Yoshinaga, K. Numata, *ACS Biomater. Sci. Eng.* **2022**, *8*, 348.
[9] H. Yu, A. Mehta, G. Wang, W. W. Hauswirth, V. Chiodo, S. L. Boye, J. Guy, *Mol. Vision* **2013**, *19*, 1482.
[10] a) S. E. Wiley, A. N. Murphy, S. A. Ross, P. Van Der Geer, J. E. Dixon, *Proc. Natl. Acad. Sci. USA* **2007**, *104*, 5318; b) A. P. Landry, H. Ding, *J. Biol. Chem.* **2014**, *289*, 4307.
[11] M. E. Tanenbaum, L. A. Gilbert, L. S. Qi, J. S. Weissman, R. D. Vale, *Cell* **2014**, *159*, 635.
[12] D. Pei, M. Buyanova, *Bioconjugate Chem.* **2019**, *30*, 273.
[13] F. Zhao, M.-H. Zou, *Front. Cardiovasc. Med.* **2021**, *8*, 749756.
[14] a) P. Somvanshi, S. Khisty, *Med. Novel Technol. Devices* **2021**, *11*, 100091; b) R. Hadianamrei, X. Zhao, *J. Controlled Release* **2022**, *343*, 600.
[15] M. Ruponen, S. Ylä-Herttuala, A. Urtti, *Biochim. Biophys. Acta* **1999**, *1415*, 331.
[16] K. A. Schug, W. Lindner, *Chem. Rev.* **2005**, *105*, 67.
[17] a) R. Truant, B. R. Cullen, *Mol. Cell. Biol.* **1999**, *19*, 1210; b) H. Brooks, B. Lebleu, E. Vives, *Adv. Drug Delivery Rev.* **2005**, *57*, 559.
[18] a) Y. Abe, T. Shodai, T. Muto, K. Mihara, H. Torii, S.-I. Nishikawa, T. Endo, D. Kohda, *Cell* **2000**, *100*, 551; b) A. Chacinska, C. M. Koehler, D. Milenkovic, T. Lithgow, N. Pfanner, *Cell* **2009**, *138*, 628; c) T. Shiota, K. Imai, J. Qiu, V. L. Hewitt, K. Tan, H.-H. Shen, N. Sakiyama, Y. Fukasawa, S. Hayat, M. Kamiya, A. Elofsson, K. Tomii, P. Horton, N. Wiedemann, N. Pfanner, T. Lithgow, T. Endo, *Science* **2015**, *349*, 1544.
[19] a) S. H. Park, A. R. Lee, K. Choi, S. Joung, J. B. Yoon, S. Kim, *BMB Rep.* **2019**, *52*, 712; b) P. Wang, D. Wang, Y. Yang, J. Hou, J. Wan, F. Ran, X. Dai, P. Zhou, Y. Yang, *Hypertens. Res.* **2020**, *43*, 1047.
[20] K. Toyooka, N. Shinozaki-Narikawa, *Microscopy* **2019**, *68*, 417.
[21] a) Y. Matsumoto, K. Itaka, T. Yamasoba, K. Kataoka, *J. Gene Med.* **2009**, *11*, 615; b) N. Yoshinaga, T. Ishii, M. Naito, T. Endo, S. Uchida, H. Cabral, K. Osada, K. Kataoka, *J. Am. Chem. Soc.* **2017**, *139*, 18567; c) N. Yoshinaga, J. K. Zhou, C. Xu, C. H. Quek, Y. Zhu, D. Tang, L. Y. Hung, S. A. Najjar, C. Y. A. Shiu, K. G. Margolis, Y.-H. Lao, K. W. Leong, *Nano Lett.* **2023**, *23*, 757.
[22] J.-A. Chuah, T. Yoshizumi, Y. Kodama, K. Numata, *Sci. Rep.* **2015**, *5*, 7751.
[23] a) J.-A. Chuah, A. Matsugami, F. Hayashi, K. Numata, *Biomacromolecules* **2016**, *17*, 3547; b) S. S. Y. Law, G. Liou, Y. Nagai, J. Giménez-Dejoz, A. Tateishi, K. Tsuchiya, Y. Kodama, T. Fujigaya, K. Numata, *Nat. Commun.* **2022**, *13*, 2417.
[24] H. Wu, G. Li, W. Chen, W. Luo, Z. Yang, Z. You, Y. Zou, *Acta Histochem.* **2022**, *124*, 151837.
[25] a) S. Pickles, P. Vigié, R. J. Youle, *Curr. Biol.* **2018**, *28*, R170; b) K. Todkar, L. Chikhi, V. Desjardins, F. El-Mortada, G. Pepin, M. Germain, *Nat. Commun.* **2021**, *12*, 1971.
[26] A. Chatterjee, E. Mambo, D. Sidransky, *Oncogene* **2006**, *25*, 4663.
[27] a) M. Su'etsugu, H. Takada, T. Katayama, H. Tsujimoto, *Nucleic Acids Res.* **2017**, *45*, 11525; b) T. Hasebe, K. Narita, S. Hidaka, M. Su'etsugu, *Life (Basel)* **2018**, *8*, 43.
[28] M. P. King, G. Attardi, *Methods Enzymol.* **1996**, *264*, 304.
[29] a) A. F. Santidrian, A. Matsuno-Yagi, M. Ritland, B. B. Seo, S. E. LeBoeuf, L. J. Gay, T. Yagi, B. Felding-Habermann, *J. Clin. Invest.* **2013**, *123*, 1068; b) C. Cortés-Rojo, M. A. Vargas-Vargas, B. E. Olmos-Orizaba, A. R. Rodríguez-Orozco, E. Calderón-Cortés, *Biochim. Biophys. Acta, Mol. Basis Dis.* **2020**, *1866*, 165801; c) N. Xie, L. Zhang, W. Gao, C. Huang, P. E. Huber, X. Zhou, C. Li, G. Shen, B. Zou, *Signal Transduction Targeted Ther.* **2020**, *5*, 227.
[30] a) M. Karbowski, R. J. Youle, *Cell Death Differ.* **2003**, *10*, 870; b) M. Picard, O. S. Shirihai, B. J. Gentil, Y. Burelle, *Am. J. Physiol. Regul. Integr. Comp. Physiol.* **2013**, *304*, R393; c) M. Giacomello, A. Pyakurel, C. Glytsou, L. Scorrano, *Nat. Rev. Mol. Cell Biol.* **2020**, *21*, 204.
[31] H. Mortiboys, K. J. Thomas, W. J. Koopman, S. Klaffke, P. Abou-Sleiman, S. Olpin, N. W. Wood, P. H. Willems, J. A. Smeitink, M. R. Cookson, O. Bandmann, *Ann. Neurol.* **2008**, *64*, 555.
[32] I. M. Artika, *Genes Dis.* **2020**, *7*, 578.

[33] a) H. Yu, V. Porciatti, A. Lewin, W. Hauswirth, J. Guy, *Sci. Rep.* **2018**, *8*, 5587; b) Y. Wang, L.-F. Hu, P.-F. Cui, L.-Y. Qi, L. Xing, H.-L. Jiang, *Adv. Mater.* **2021**, *33*, 2103307.
[34] L. Jiang, S. Zhou, X. Zhang, C. Li, S. Ji, H. Mao, X. Jiang, *Nat. Commun.* **2021**, *12*, 2390.
[35] A. J. Afolayan, R.-J. Teng, A. Eis, U. Rana, K. A. Broniowska, J. A. Corbett, K. Pritchard, G. G. Konduri, *Am. J. Physiol* **2014**, *306*, L351.
[36] a) K. P. Künkele, S. Heins, M. Dembowski, F. E. Nargang, R. Benz, M. Thieffry, J. Walz, R. Lill, S. Nussberger, W. Neupert, *Cell* **1998**, *93*, 1009; b) K. Hill, K. Model, M. T. Ryan, K. Dietmeier, F. Martin, R. Wagner, N. Pfanner, *Nature* **1998**, *395*, 516.
[37] A. Gupta, T. Becker, *Biochim. Biophys. Acta, Bioenerg.* **2021**, *1862*, 148323.
[38] a) Y. Miyamoto, N. Kitamura, Y. Nakamura, M. Futamura, T. Miyamoto, M. Yoshida, M. Ono, S. Ichinose, H. Arakawa, *PLoS One* **2011**, *6*, 16054; b) X. Zhang, X. Zuo, B. Yang, Z. Li, Y. Xue, Y. Zhou, J. Huang, X. Zhao, J. Zhou, Y. Yan, H. Zhang, P. Guo, H. Sun, L. Guo, Y. Zhang, X.-D. Fu, *Cell* **2014**, *158*, 607; c) L. Ruan, C. Zhou, E. Jin, A. Kucharavy, Y. Zhang, Z. Wen, L. Florens, R. Li, *Nature* **2017**, *543*, 443; d) P.-L. Chen, K.-T. Huang, C.-Y. Cheng, J.-C. Li, H.-Y. Chan, T.-Y. Lin, M. P. Su, W.-Y. Yang, H. C. Chang, H.-D. Wang, C.-H. Chen, *Nat. Commun.* **2020**, *11*, 2592.
[39] D. Lechardeur, K.-J. Sohn, M. Haardt, P. B. Joshi, M. Monck, R. W. Graham, B. Beatty, J. Squire, H. O'brodovich, G. L. Lukacs, *Gene Ther.* **1999**, *6*, 482.
[40] A. Stoccoro, F. Coppedè, *Int. J. Mol. Sci.* **2021**, 22.
[41] Z. Lei, H. Meng, L. Liu, H. Zhao, X. Rao, Y. Yan, H. Wu, M. Liu, A. He, C. Yi, *Nature* **2022**, *606*, 804.
[42] P. A. Gammage, C. T. Moraes, M. Minczuk, *Trends Genet.* **2018**, *34*, 101.